

Microstructural regimes of colloidal rod suspensions, gels, and glasses

Michael J. Solomon^{*a} and Patrick T. Spicer^{*b}

Received 3rd September 2009, Accepted 4th January 2010

First published as an Advance Article on the web 2nd February 2010

DOI: 10.1039/b918281k

We review the diverse range of materials made up of rod-shaped colloids. A common feature of such suspensions is the strong and efficient contribution of rods to the material's solid-like rheological properties such as elastic modulus and yield stress. Colloidal rod suspensions span from biomaterials such as f-actin and fd virus to inorganic materials such as boehmite and hematite, and to commercial fibers such as cellulose. We argue that, depending on the strength of pair potential interactions, such rod suspensions form microstructures that vary between the two limits of heterogeneous fractal clusters and homogeneous fiber networks. The volume fraction range for transition between these two limiting cases is strongly aspect ratio dependent. The two limiting microstructures can be distinguished by differences in the scattering vector dependence of their structure factors, as long as the range of scattering vector probed is sufficient to span regimes both above and below $qL \approx 1$. Here q is the scattering vector and L is the rod length. Theories of the Brownian dynamics of fractal clusters and fiber networks show that the two types of microstructure can lead to the arrested dynamics of gelation and the glass transition, respectively. The volume fraction and aspect ratio dependences of the dynamical slowing down of these two cases differ significantly; we suggest that probing these differences is a convenient way to distinguish between gels and glasses of colloidal rods. This distinction is important to clarify because these microstructures are determinants of rheological properties such as elasticity and yielding. By combining these structural and dynamical ideas about rods, we classify a set of literature measurements on more than fifteen different colloidal materials and thereby distinguish between regimes of gelation and vitrification. We conclude by suggesting directions for future research in the arrested dynamics, the non-linear rheology, and the absolute lower limit of gelation in colloidal rod suspensions.

1 Introduction

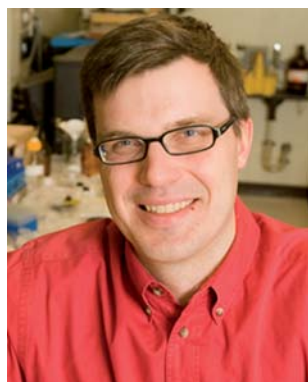
Many classes of soft matter microstructures exhibit a tailored rheological response because of the interaction of rods. For example, networks of actin filaments and microtubules produce

the mechanical response of the cytoskeleton.^{1,2} Carbon nanotube^{3,4} or natural fiber⁵ networks produce a static modulus that affects the performance of polymeric composites. Pulp and paper fiber networks^{6,7} yield the mechanical integrity that is a prerequisite for processing and press performance. Magneto- and electrorheological fluids may also include rod particles.^{8,9}

In these materials the basic building block¹⁰ that yields the rheological response is a rod-shaped microscopic particle. Whether a pulp fiber, a wax crystal, or an actin filament, the

^aDept. of Chemical Engineering, University of Michigan, Ann Arbor, MI, 48109, USA. E-mail: mjsolo@umich.edu

^bCorporate Engineering, Procter and Gamble Co., West Chester, OH, 45069, USA. E-mail: spicer.pt@pg.com



Michael J. Solomon

Michael J. Solomon is Professor of Chemical Engineering at the University of Michigan Ann Arbor. His research interests are in colloidal gelation and rheology as well as the assembly and dynamics of anisotropic particles. His group uses methods in confocal microscopy and light scattering to investigate these areas.



Patrick T. Spicer

Patrick T. Spicer is a Technical Section Head in the Microstructured Fluids group at the Procter & Gamble Company in Cincinnati, Ohio. His group focuses on engineering research and development via collaborative projects with P&G business units and academic groups.

properties that are most germane to the rheological response of these materials are the anisotropic excluded volume of the particle and the colloidal forces that the particles exert on their surroundings. The dimensions of the rod building blocks of these materials vary widely; however, characteristic sizes from ~ 1 nm to $10 \mu\text{m}$, the domain of soft matter, are very common. Fig. 1 summarizes the tremendous diversity of soft materials that are comprised of rod-shaped particles. The characteristic size of the rods varies from molecular-scale rigid rod polymers, such as xanthan gum,¹¹ which are used as food additives, to colloidal metal oxide rods, which are used in magnetic storage^{12–14} as well as shear-thickening materials,¹⁵ to granular fibers, which are used in composites or paper pulp.⁶

Granted microstructures comprised of spheres, plates, and discs are also well represented in soft matter. Nevertheless, the scope of Fig. 1 makes clear that rod shape is a key foundation for generating soft matter rheological response. The rod structures shown in Fig. 1 are drawn from a diverse literature spanning multiple, partially overlapping areas as well as three orders of magnitude in aspect ratio. This review will address the question of what can be learned about the microstructure and rheology of these materials by considering them within a common

framework. Unifying these different literatures is useful because the amount of fundamental study they have enjoyed varies widely, as does the degree of commercial interest in the different materials. To understand this variation, consider the three examples of actin (Fig. 1f), organo and hydrogelators (Fig. 1n and o), and cellulosic natural fibers (Fig. 1e), in more detail.

Actin polymerizes in multiple modes to form the structural framework of our cells, providing elasticity and mechanical integrity to the bodies of living creatures and even propelling them in some cases.¹⁶ The study of actin biopolymer yields insight into cell mechanics¹⁷ and the mechanisms of rod dispersion rheology. Actin has been principally modeled by extensions of dilute and concentrated polymer rheology¹⁸ to account for semi-flexibility, bending moments, and glassy dynamics.^{19–23} Other biomaterials such as tobacco mosaic or fd virus are also excellent monodisperse model rod systems that, because of their rich equilibrium phase behavior,²⁴ have been used to test theoretical models of liquid crystallinity.²⁵

The gelation of oil or water systems using, respectively, organogelators or hydrogelators is an important area of rod dispersion research that balances fundamental and applied concerns. Examples of gelator compounds include hydroxystearic acid²⁶

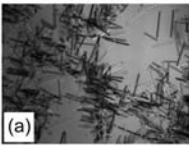
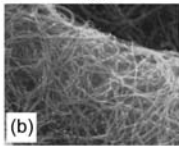
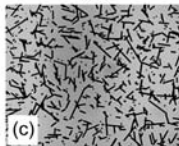
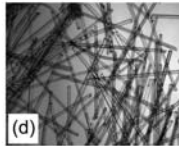
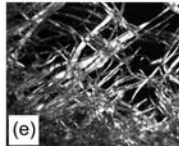
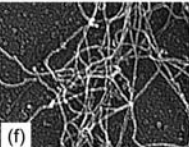
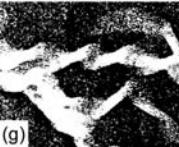
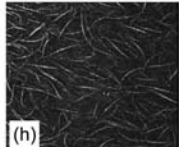
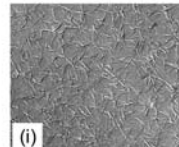
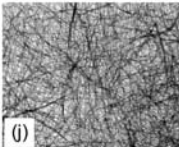

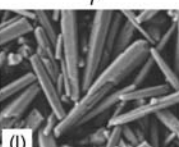
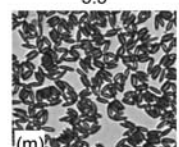
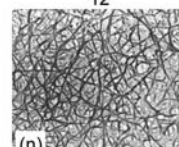
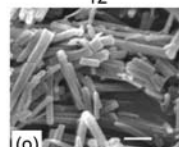
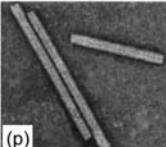
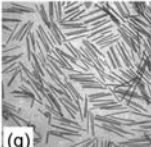

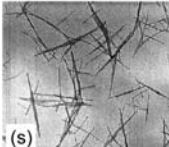
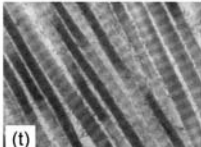
Granular	Rayon L = 100 μm r = 10	C nanotube (32) 150 μm 150	Ni-coated C 200 μm ~ 25	Acrylic fibers 700 μm ~ 50	Cellulose ~ 1 mm 500	
						
	(a)	(b)	(c)	(d)	(e)	
	Colloidal	Actin (16) L $\sim 10 \mu\text{m}$ R = 500	Calcium soap (117) 10 μm 166	Polyamide (91) 26 μm 306	Polyethylene wax 25 μm 15	Bacterial Cellulose 50 μm 100
						
(f)		(g)	(h)	(i)	(j)	
Hematite (121) L = 1 μm r = 3		CaCO ₃ (15) 1 μm 7	Polystyrene (116) 3 μm 5.5	Organogelator (123) 4 μm 12	Hydrogelator (119) 4 μm 12	
						
(k)	(l)	(m)	(n)	(o)		
Nanoscale	TMV (122) L = 300 nm r = 8.3	Gold (120) 500 nm 25	SiO ₂ (124) ~ 700 nm ~ 100	Boehmite (99) 900 nm 30	Collagen (118) ~ 900 nm ~ 200	
						
	(p)	(q)	(r)	(s)	(t)	

Fig. 1 Examples of rod colloids spanning four orders of magnitude in length and three orders of magnitude in aspect ratio.^{15,16,32,91,99,116–124} The diverse sources, research areas, and applications of these materials emphasize the broad need for more fundamental understanding of rod gels and the importance of unifying the literature of this field under a common framework. Images reprinted with permission from the indicated references. Images a, c–e, and i by one of the authors (P.S.).

and gemini surfactants.²⁷ These systems usually form gels from self-assembled and/or crystallized rod structures. These structures can be cross-linked or non-interacting depending on their chemistry²⁸ and whether they are used in cosmetics,²⁹ greases,²⁶ or paints.³⁰ Characteristic structural features of gelator rods can span multiple decades because molecular-scale fibril micelles may hierarchically assemble into colloidal fiber and rod structures.²⁷ Most published work focuses on gelator chemistry; comprehensive rheological studies of these materials are less common.^{31,32}

As a final example, consider that natural cellulose fibers, a rod-shaped particle, are a key component of material performance in the high-volume application of pulp and papermaking. Motivated by its value as a raw material, rheological research in paper pulp networks and rheology is widespread.^{6,7} An emerging application of cellulosic materials is as a constituent of biomass that is enzymatically processed for biofuels.³³

While rod suspensions of actin, gelators, and cellulose appear nearly unrelated from the point of view of both applications and attention paid to their fundamental physics, these systems and their microstructural effects on rheology are linked by the commonality of their rod-shaped building blocks. In this review we present a unifying framework within which the gelation, vitrification and rheology of the diverse material classes of Fig. 1 may be addressed. We argue that the common features of rod anisotropy and colloidal microstructure connect the materials in Fig. 1 and that their rheology, particularly whether they will display the solid-like viscoelasticity of gels and glasses, can thus be described on this universal basis. We suggest that rod microstructure can be modeled along a spectrum that spans from one limiting case of fractal clusters to another limiting case of homogeneous rod networks. These cases correspond to two limits for the onset of slow dynamics—rod gels and rod glasses—that are important to most applications of the materials of Fig. 1. We conclude by investigating how literature studies of the Fig. 1 materials fit into the spectrum of possible arrested gel and glass structures. We furthermore identify questions for further development given the increasing commercial and research importance of rod colloids.

2 Common features of rod suspensions

For applications, a common research aim is to predict rod dispersion rheological response from underlying physicochemical properties in order to correlate processing and stability characteristics of product formulations with rheological behavior. Rheological properties of interest are the linear viscoelastic moduli, $G'(\omega)$ and $G''(\omega)$, the shear-rate dependent viscosity, $\eta(\dot{\gamma})$, and the yield stress, τ_y . The linear viscoelastic moduli are a function of the unperturbed (quiescent) suspension microstructure while the non-linear rheological properties such as the viscosity and yield stress require explicit consideration of flow effects on microstructure.³⁴ The fluid-phase microdynamics and rheology of rigid rod suspensions have been investigated in a number of contexts, particularly in the areas of rigid rod polymers^{18,35–41} and in the hydrodynamics of fiber suspensions.^{42–47} The rheological behavior of ordered solutions of rigid rods has also been addressed.^{48–51}

In this review we focus on the origin of solid-like rheology of rod suspensions, since such elasticity is crucial to many complex fluid and soft matter applications. The principal way to generate

a significant level of elasticity in colloidal suspensions is to arrest particle dynamics at the microscopic level. There are multiple kinds of structures that can result in microscopic dynamic arrest. For suspensions of spheres, gels are taken as materials with slow dynamics due to attractive interactions and bonding; glasses are materials with slow dynamics due to excluded volume interactions and packing.^{52,53} We adopt the same terminology for rod suspensions. We are particularly interested in the physical and colloidal properties that lead to gelation or vitrification, since, as we will see, the underlying microstructures linked to these two kinds of slow dynamics are so different.

How are these gel and glass definitions typically linked to the application requirements of a colloidal rod formulation? An example is the production of carbon nanotube composites, which requires the dispersion of colloidal unstable multi-walled carbon nanotubes in highly viscous polymer melts. Such rod dispersions must flow at low shear stresses. These constraints require a quiescently formed network to rapidly break down and then re-gel upon cessation of flow.⁵⁴ Phenomena such as percolation, phase stability, aggregation, flexibility and polydispersity have all been found to affect performance.^{4,55–60} Such needs, constraints and behavior are identical to those of liquid consumer products. These materials use colloidal rod gels to suspend dispersed phases like emulsion droplets: liquid soap and shampoo processing requires resilience to shear stress during transport but rapid restructuring is also necessary once the product is in the bottle. The same product must flow easily when a consumer dispenses it, but then regain its structure and stability once application ends and the product is stored. In terms of numerical magnitudes, typical requirements are small yield stresses (~ 0.5 Pa) and short structural recovery times (~ 1 min).

Thus, although the composition and chemistry of the rod suspensions in Fig. 1 vary considerably, they share the common feature of the colloidal scale. Given that the rod length is such that the suspension is in the colloidal domain,⁶¹ four key physicochemical properties control the microstructure, dynamics and rheology of rod-containing materials at this scale: (i) interparticle forces; (ii) aspect ratio; (iii) particle number density; and (iv) flexibility.

Interparticle forces

Rod suspensions are typically prepared at a number density in which contacts between rods are common—indeed, as discussed earlier, it is such jammed or gelled states that generate the mechanical properties of ultimate interest for applications. Rod contacts may involve charge, dispersion, or depletion forces, and/or frictional interactions. Such interparticle forces are a determinant of the structural heterogeneity of the rod network. Possible structures, as considered in the next section, range from homogeneous networks of non-interacting rods to heterogeneous fractal clusters in cases where the rods are strongly interacting. The strength of interparticle forces in rod suspensions may be parameterized by the dimensionless quantity $U_{\text{contact}}/k_{\text{B}}T$, where U_{contact} is a characteristic pair potential energy of two rods at contact and $k_{\text{B}}T$ is the energy scale of thermally induced Brownian forces. Although the pair potential is a function of separation and orientation, interactions in rod dispersions are often short-ranged, especially relative to the rod length, L . The contact

potential (or, alternatively, the second virial coefficient) is a useful characteristic quantity in this case.

Thus, the limit $U_{\text{contact}}/k_{\text{B}}T \ll 1$ corresponds to the case of non-interacting rods. $U_{\text{contact}}/k_{\text{B}}T \gg 1$ corresponds to strongly interacting rods that are more likely to display irreversible kinetics such as diffusion-limited cluster aggregation (DLCA). Intermediate values, $U_{\text{contact}}/k_{\text{B}}T \approx 1$, lead to effects such as weak aggregation, transient gelation and/or phase separation. This intermediate range of potentials, best studied for the cases of thermoreversible and polymer depletion interactions, is of great importance to the assembly of orientationally ordered phases.^{62–67} Yet, practically, the isotropic phase of rods is very commonly encountered and this case can be accessed in either the strongly ($U_{\text{contact}}/k_{\text{B}}T \gg 1$) or weakly interacting ($U_{\text{contact}}/k_{\text{B}}T \ll 1$) limits. Thus, the precise control of interactions required to generate $U_{\text{contact}}/k_{\text{B}}T \approx 1$ is not a necessary condition for the practical application of the materials shown in Fig. 1.

Aspect ratio

The anisotropic excluded volume of rods affects their amorphous packing and phase stability. Brownian translational and rotational dynamics are a strong function of the rod length.¹⁸ At the particle level, shape is typically modeled as either that of a prolate spheroid or a cylinder with hemispherical end caps. Rod shape has also been described as acicular or needle-like. Although the small differences between these geometries can affect the location of order–disorder transitions of liquid crystal phases^{68,69} at small aspect ratios, as can polydispersity,⁵⁶ the amorphous and gel structures that are of interest to this review are less sensitive to such fine shape details, particularly at high aspect ratio. In this case it is the ratio of rod length, L , and width, b , the aspect ratio, $r = L/b$, that determines the effect of excluded volume interactions on microstructure.

Number density

Along with aspect ratio and pair interactions, number density, ρ , completes the set of parameters that controls the microstructure of rigid rods. Here ρ is proportional to the volume fraction ϕ ; $\phi = \rho V_{\text{p}}$ where V_{p} is the rod particle volume (e.g. $V_{\text{p}} = (1/6)\pi Lb^2$ for a prolate spheroid; $V_{\text{p}} = (\pi/4)Lb^2 + (\pi/8)b^3$ for a cylinder with spherical end caps). In the non-interacting limit, there are three concentration regimes.¹⁸ For $\rho \ll 1/L^3$ ($\phi \ll 1/r^2$), the rods are dilute and rarely interact, either structurally or dynamically. In the semi-dilute range, $1/L^3 \ll \rho \ll 1/bL^2$ ($1/r^2 \ll \phi \ll 1/r$), each rod has few structural contacts with its neighbors but suspension Brownian dynamics are a strong function of number density. This strong dependence arises because particle rotations are hindered as a consequence of the fact that the mean separation between rods is less than the rod's length. Finally, in the isotropic concentrated regime, $\rho \gg 1/bL^2$ ($\phi \gg 1/r$), rod rotation is severely hindered by strong structural correlations and multiple, random inter-rod contacts. Concentrating a rod system into this range also yields the order–disorder transitions of liquid crystals.^{24,70,71} Greater concentrations still yield phases with both positional and orientational order, as well as close-packed limits.^{68,69,72,73} These limiting concentration regimes are routinely applied to classify rigid rod polymer solutions. The extension to

rigid rod colloids is straightforward; however, implicit in these expressions is the assumption of $U_{\text{contact}}/k_{\text{B}}T \ll 1$. For example, the concentrated isotropic rod solution limit, $\rho \gg 1/bL^2$, arises from the scaling of the excluded volume interaction of two rods. Because many of the structures in Fig. 1 are formed from strongly interacting rods, the typical division into dilute, semi-dilute and concentrated isotropic regimes requires refinement in these cases.

Flexibility

In addition to the three attributes described above for rigid particles, the rods of Fig. 1 may also vary from fully rigid to semi-flexible. Flexibility is characterized by the length ratio L/l_{p} , where l_{p} is the persistence length, a quantity that can be extracted from, for example, static light scattering⁷⁴ or direct visualization measurements.⁷⁵ (The persistence length is the distance along the contour of a rod for which the ensemble-averaged, mutual orientation of two points first becomes decorrelated.) Thus, for rigid rods, $L/l_{\text{p}} \ll 1$, while for semi-flexible filaments, $L/l_{\text{p}} \approx 1$. Although it is clear that low-aspect ratio particles comprised of inorganic materials such as boehmite or hematite fall in the rigid limit, nanotubes and cellulose fibers may show semi-flexible behavior when sufficiently long. For example, the persistence length of single-walled carbon nanotubes has been reported to be $l_{\text{p}} \approx 30\text{--}170 \mu\text{m}$.⁷⁵ This quantity is also diameter dependent.⁵⁵ Biopolymers such as actin display the effects of semi-flexibility, particularly in their high frequency rheology.^{19,20} This rheological response at high frequencies is a function of the bending modulus or rigidity, κ , which is dependent on the persistence length ($\kappa = l_{\text{p}}k_{\text{B}}T$).¹⁸

3 Structural models: heterogeneous fractal clusters and homogeneous fiber networks

Classical discussions of rod suspensions were motivated by interest in rigid rod polymer solutions, colloidal liquid crystals, and molecular liquids. Although the effect of pair interactions has been addressed,^{63,66,76,77} the effects of excluded volume repulsion are the principal determinant of the equilibrium phase behavior. In this case, $U_{\text{contact}}/k_{\text{B}}T = 0$ and the rod density is spatially homogeneous in the sense that the mean size of any voids and clusters is limited to dimensions less than the rod length, L . However, many practical systems differ from this case in one of two ways. First, the rod density may be spatially heterogeneous on scales greater than L because of strong attractive interactions ($U_{\text{contact}}/k_{\text{B}}T \gg 1$). Second, the rod particles may be semi-flexible. In the first case, strong attractive interactions induce aggregation. At the dilute volume fractions typical of rod applications such as stabilization, rod fractal clusters result. For colloids, the measured fractal dimension from diffusion-limited cluster aggregation is a strong function of aspect ratio,⁷⁸ varying from $D \approx 1.8$ for spheres to $D \approx 2.2$ for rods of aspect ratio 30. In the second case, flexibility effectively decreases the rod's radius of gyration, thereby increasing the rod's diffusivity and intrinsic viscosity as well as affecting relaxation at high frequencies.¹⁸

A convenient way to quantify the effects of attractions and flexibility on rod suspension microstructure is by means of

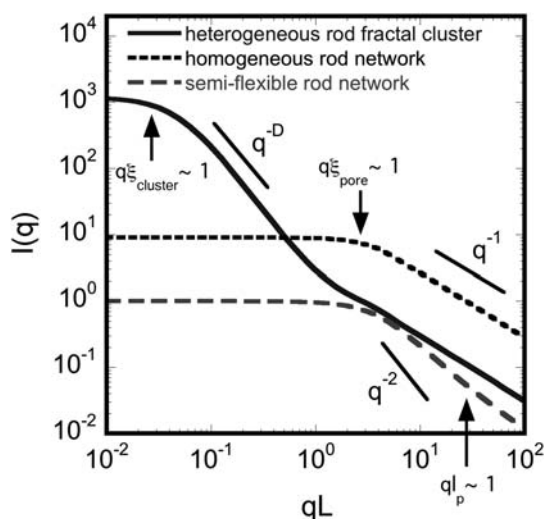


Fig. 2 Comparison of the q -dependent scattering intensity, $I(q)$, for the limiting cases of rod suspension structure: homogeneous rigid rod networks and heterogeneous rod fractal clusters. The effect of semi-flexibility on scattering from the homogeneous network is also plotted. The rigid and semi-flexible homogeneous rod network scattering are each shown for the particular case of $\xi_{\text{pore}}/L = 0.5$. For the semi-flexible network, $l_p/L = 0.05$. For the heterogeneous fractal clusters, $\xi_{\text{cluster}}/L = 20$ and $D = 2.1$, consistent with literature measurements for $r \approx 10$. Scattering form factors are computed in the Rayleigh–Debye approximation. Structure factors are computed from the models of Chen and Teixeira⁸⁸ and Schurtenberger *et al.*⁸¹ The three curves are offset on the ordinate for clarity.

scattering measurements. Depending on the size of the rod building block, X-ray, neutron, and light scattering are potentially applicable. Fig. 2 plots scattering behavior computed for the limiting cases of heterogeneous rigid rod fractal clusters, homogeneous rigid rod networks and homogeneous semi-flexible rod networks. The measured scattering intensity, $I(q)$, is a function of the scattering vector $q = (4\pi/\lambda)\sin(\theta/2)$ where λ is the wavelength of the radiation in the scattering medium and θ is the scattering angle. Qualitatively, scattering at some scattering vector q^* occurs by interaction of radiation with structural features of size l^* where $l^* \approx 2\pi/q^*$. $I(q)$ is the product of the number density of scatterers, the scattering from an individual particle, and the scattering due to the effect of collective structure. Thus, $I(q) = \rho F(q)S(q)$ where ρ is the number density, $F(q)$ is the form factor of a single particle, and $S(q)$ is the structure factor, a measure of the effect of collective structure. The structure factor quantifies pair correlations. For a suspension with isotropic structure such as we consider here, $S(q) = 1 + 4\pi\rho \int dr r^2 \frac{\sin qr}{qr} (g(r) - 1)$ where $g(r)$ is the radial distribution function. In Fig. 2 we plot $I(q)$ for the particular case of rods whose form factor, $F(q)$, can be described by Rayleigh–Debye theory. In this theory, the form factor, $F(q)$, of a randomly oriented suspension of rods scales as q^{-1} for large qL .^{79,80}

Of the three systems, $I(q)$ for the homogeneous rigid rod network shows the simplest behavior. In this case, the only structural feature is a characteristic pore size, ξ_{pore} of the network, where $\xi_{\text{pore}} < L$. ξ_{pore} decreases with concentration. Thus, as q decreases, the scattering crosses over from a q^{-1} to

a Guinier dependence. This crossover tracks a change from a regime in which scattering from single rods dominates (at high q) to one in which collective effects dominate (at low q). At low q , $I(q) \approx 1 - (q\xi_{\text{pore}})^2$.^{81,82}

If the homogeneous network is instead comprised of semi-flexible rods, then additional functionality is apparent in $I(q)$.⁸¹ The $qL > 1$ scattering of a semi-flexible rod network displays two scaling regimes. In addition to the q^{-1} regime characteristic of the rod geometry, a q^{-2} regime characteristic of a Gaussian coil is observed if $L < l_p < b/2$. The crossover between these two regimes is at $ql_p \approx 1$. Just as for the rigid case, semi-flexible rod networks are characterized by a pore size that can be extracted from the low q scattering of the Guinier regime.

Since $F(q)$ tends to unity for $qL \ll 1$, the low q regime is dominated by the behavior of $S(q)$. In this regime, over large q ranges, power-law scattering in a variety of rod suspensions has been observed.^{78,80,83–87} This scaling is characteristic of scale invariant, fractal structure. In this case, $I(q) \approx q^{-D}$ where D is the fractal dimension of the aggregate. For example, for diffusion-limited cluster aggregation, $D \approx 2.1$ for rods of aspect ratio ~ 10 . Both experiment and simulation indicate that the value of D varies with aspect ratio.⁷⁸ This regime spans from $q\xi_{\text{cluster}} \approx 1$ to $qL \approx 1$. At $q\xi_{\text{cluster}} \approx 1$, the scattering is expected to crossover to a low- q plateau that reflects the finite size of the fractal clusters.⁸⁸ For fractal clusters, the cluster size is typically a decreasing function of the bulk volume fraction.⁸⁹

Although the general proposal to classify rod structures on a continuum between fractal clusters and homogeneous networks appears reasonable, this scheme does implicitly assume orientational isotropy of the rods. Yet, at number densities $\rho^* \approx bL^2$ (or equivalently $\phi^* \approx b/L \approx r^{-1}$), an equilibrium phase with orientational order appears.^{18,24,71} However, as we discuss in the next section, concentration ranges for which elastic, solid-like rheology are commonly observed appear well below the nematic transition.

Thus, Fig. 2 provides a basis for characterizing rod microstructure from q -dependent scattering. In conclusion, we caution that a number of additional factors might complicate the general application of this approach. First, if the rod length is poorly characterized or if results are not scaled on qL , then distinguishing between the fractal scaling of aggregated systems and the q^{-2} scaling of semi-flexible networks could be difficult.^{83,85,87} We in particular note that the function plotted for the semi-flexible rod network in Fig. 2 has also commonly been applied to polymer-like materials such as micellar solutions. The structural signatures of these materials, if present, could easily be confused with that of rods, especially if some flexibility in the rods is possible.⁸¹ Second, for large diameter rods, additional functionality in the scattering may be apparent at dimensionless scattering vectors $qb > 1$, where b is the rod diameter.⁸⁰ These regimes would be most likely observed by means of neutron and X-ray scattering. Third, particle polydispersity could obscure the crossovers that occur at $q\xi_{\text{cluster}} \approx 1$ and $q\xi_{\text{pore}} \approx 1$. Fourth, for small aspect ratios, the scattering vector ranges for which the different regimes would be observed might be limited. Finally, hierarchical structures might exist. For example, local nematic order on small scales might be integrated with structures that are isotropic on large scales. Such hierarchical structure, and associated kinetic pathways,⁹⁰ would further complicate the use of

scattering to classify structure. Examples of systems with hierarchical structure include those that exhibit bundling, such as polyamide rods with depletion attractions,⁹¹ and nematic gels.^{62,65}

4 Microstructural components of the dynamical and rheological response

The structural differences between homogeneous rod networks and heterogeneous rod fractal clusters highlighted in Fig. 2 have implications for the dynamical and rheological response of rod suspensions. For rod suspensions that interact through pair potentials and experience Brownian motion, the linear rheology and suspension dynamics are strongly connected, as demonstrated by approaches such as microrheology.⁹² Moreover, the single-particle translational and rotational diffusivities of a suspended rod are a consequence of the rod's local structural environment. Two local structural environments, one characteristic of rod networks and the other of rod fractals, are shown in Fig. 3a and b. In the homogeneous rod network (Fig. 3a), at its most concentrated, rods have ~ 10 nearest neighbors.⁹³ (The maximum number of nearest neighbors that avoid the isotropic–nematic transition in equilibrated systems is about seven.) The orientation distribution of these rods is isotropic and the pore space between rods is much less than the rod length, L . In contrast, fractal clusters of rods formed by diffusion-limited cluster aggregation (DLCA) represent a limiting case of just two contacting neighbors (Fig. 3b). Here also the distribution of rod orientations is isotropic. If the volume fraction is low, the fractal structure implies the existence of voids in the suspension that are larger than the rod length.⁸⁹ Rod suspensions with arrested dynamics, as would be of interest for rheological modification, fall intermediate between these two scenarios. Such intermediate structures could be achieved *via* two different approaches. One possibility would be to reduce the concentration of a homogeneous rod network, such as shown in Fig. 3a, so that the mean contact number fell to less than seven. Added pair attractions

would stabilize the network, although re-entrant phenomena could complicate this simple picture. Alternatively, kinetic processes like aging could lead to local rearrangements of irreversibly aggregated structures. These processes would increase the contact number of DLCA fractal structures, such as shown in Fig. 3b, above two.

Implicit in Fig. 3a and b is a difference in pair interactions: $U_{\text{contact}}/k_{\text{B}}T \ll 1$ for Fig. 3a, while $U_{\text{contact}}/k_{\text{B}}T \gg 1$ for Fig. 3b. That is, the neighboring rods shown in Fig. 3 may constrain single-rod dynamics due to the effects of their excluded volume (due to packing^{23,94,95}) and/or pair potential interactions (due, for example, to attractive van der Waals or depletion forces).⁹⁶ Hydrodynamic interactions between rods may also play a role.^{38,40,46} As the effects of packing or attractive interactions on dynamics increase, single-rod dynamics may be retarded to the point that rods are effectively localized on scales on the order of the rod diameter. At this point, arrested dynamics will lead to effects such as non-ergodicity and elasticity. Consistent with the literature for spheres, we refer to arrested systems resulting from packing and excluded volume interactions (as shown in Fig. 3a) as rod glasses. Rod gels are then systems in which arrested dynamics occur due to bonding between rods due to attractions, as per structures such as Fig. 3b. Both gels and glasses differ from suspensions by their non-ergodicity, which is observable by methods such as dynamic light scattering.⁹⁷

As is the case for spheres,^{52,53} the two limiting cases of attractive gels (low-volume fraction, strong attractions) and hard-rod glasses (high-volume fraction, no attractions) are thought to be connected by a set of arrested structures that are intermediate in volume fraction and pair interactions. However, because of the additional parameter of aspect ratio, the set of possible combinations of structure and dynamics available for designed response is very great, as discussed in Section 3.

Using the structures shown in Fig. 3a and b, simple models of single-rod diffusion can be applied to clarify the transition to arrested dynamics, distinguish between dynamical characteristics of gels and glasses, and identify effects of aspect ratio. Edwards and Evans⁹⁵ considered the diffusion of a test rod in a hard-rod network. A key result of their work is that the excluded volume effects of neighboring rods begin to significantly retard single-rod translational diffusion at volume fractions $\phi \approx r^{-1}$. The diffusivity, scaled on the result for a free rod, is:

$$\frac{D(\phi)_{\text{network}}}{D_0} = 1 - C \left(\frac{4\phi r}{\pi} \right)^{3/2} \quad (1)$$

The functional form, particularly the scaling power of 3/2, leads to an abrupt onset of arrested dynamics, as plotted in Fig. 3c for the characteristic aspect ratios of 4, 9, and 30. The glass transition is progressively shifted to lower volume fractions with increasing aspect ratio. The origin of this shift rests with the characteristic scaling $\phi_{\text{glass}} \approx r^{-1}$. (Note that the particular values of ϕ_{glass} at each aspect ratio are determined by the magnitude of C in the equation.) It is significant that the aspect ratio dependence of the rod glass transition implied by eqn (1) is identical to the scaling of the isotropic–nematic phase transition. Thus, vitrification and equilibrium nematic order in hard rods are expected to occur in approximately the same range of colloid volume fractions.

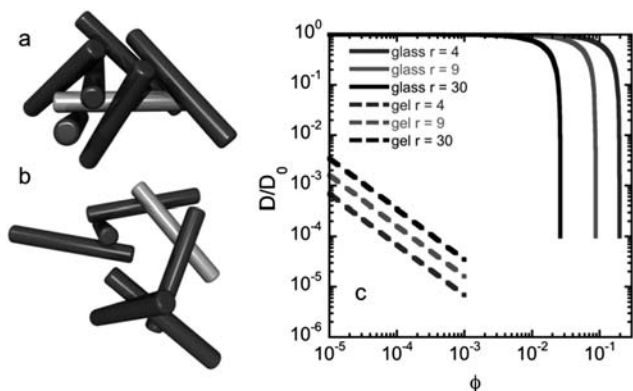


Fig. 3 Effect of suspension structure on rod dynamics. The volume fraction dependent self-diffusivity for suspensions of rods with $r = 4, 9$ and 30 is estimated from the theories of Edwards and Evans⁹⁵ (eqn (1) with $C = 1$) and Krall and Weitz⁹⁸ (eqn (2)). Parameters for fractal clusters are taken from dynamic light scattering measurements of colloidal boehmite.⁹⁹ D_0 is the translational diffusivity of a rod at infinite dilution.¹⁸

To illustrate arrested dynamics in fractal structures of rods, consider the model for internal dynamics of fractal clusters due to Krall and Weitz.⁹⁸ A key feature of this model is stretched exponential dynamics. These dynamics are increasingly retarded as volume fraction increases because internal cluster dynamics become increasingly localized. Because fractals are scale-invariant structures, the exact details of the monomer shape are not key to this description, so we here apply the model to investigate the dynamics of structures such as that shown in Fig. 3b. (Indeed, the model describes the time-dependence of the dynamic structure factors of rod gels very well,⁹⁹ however, the volume fraction dependence of model parameters is significantly different from spheres.) To facilitate comparison to the dynamics of rod glasses, we construct an effective diffusivity from a characteristic localization length and fluctuation time of this model. In this case:

$$\frac{D(\phi)_{\text{fractal}}}{D_0} = \frac{\delta^2(\phi)}{6\tau(\phi)} \left(\frac{1}{D_0} \right) \quad (2)$$

where $\delta^2(\phi)$ is the maximum mean-squared displacement of rods in the fractal cluster and $\tau(\phi)$ is the relaxation time of the initial decay constant in the dynamic structure factor. To illustrate behavior we assign the parameters of eqn (2) from the measurements of Mohraz and Solomon⁹⁹ for boehmite rod gels ($r = 4, 9$ and 30) whose measured structure factors were consistent with fractal scaling⁷⁸ as per the theories discussed in Section 3. As for the case of rod glasses, rod fractal gels exhibit retardation in dynamics as volume fraction is increased. However, the scaling of dynamics obeys a more gradual power-law in ϕ , rather than the abrupt downturn observed for the rod glass. The power-law behavior in ϕ is consistent with the underlying fractal structure. Thus, for rod fractal gels, there is no abrupt transition to arrested dynamics, as predicted by the Edwards and Evans theory⁹⁵ of packing effects on rod diffusion. Fig. 3c yields predictions about rod gelation and vitrification that could be explored by experiment, including the volume fraction scaling of the two transitions with aspect ratio. The particular functional forms of the volume fraction dependent dynamics of rod glasses and gels have likewise yet to be examined by experiment. Finally, just as discussed in the previous section on structure, the two different signatures of dynamical arrest reported in Fig. 3 represent limiting cases. Inspection of Fig. 3 shows that rod fractal gels and homogeneous network glasses are separated by orders of magnitude in volume fraction. The effect of rod anisotropy, as parameterized by aspect ratio, is to shift gelation and vitrification points in a way that provides an additional tool to design solid-like rheology. We discuss the implications of this shift in the next section.

5 Geometric commonalities of rod networks

Because broadly applicable models relating microstructure to rheology in rod suspensions are currently lacking, it is valuable to investigate commonalities among the different rod systems in Fig. 1. One unifying feature of rod systems is their seeming ability to form space-filling networks and efficiently create elasticity and a solid-like rheological response at lower volume fractions than more isotropic shapes. This advantage of rods is economically

significant for commercial applications like composite materials and consumer products.^{100,101}

To examine this feature, in Fig. 4 we plot the volume fraction and aspect ratio of a number of rod suspensions whose elastic, solid-like rheology has been reported in the literature. The data in Fig. 4 include experimental results that span the nanometre, colloidal, and granular length scales and which are drawn from a diverse range of materials, applications, and disciplines. All data have been selected as examples where the formation of a network is directly measured or inferred by bulk behavior such as the existence of a yield stress. In some cases, authors reported volume fractions calculated geometrically, while others accounted for ionic and excluded volume effects, while some reported mass fractions that we converted to volume fractions by estimating material properties such as density. Also shown in Fig. 4, at $r = 1$ on the y -axis, are representative data for gels and glasses of colloidal spheres. Fig. 4 offers a holistic picture of geometric packing limits for a broad range of rod microstructures. It is subject to the limitation that pair potential interactions are not explicitly mapped; this extension would require a three-dimensional space of volume fraction—aspect ratio—pair potential. Nevertheless, we recommend that it be used to rationalize and design rod microstructures from materials of interest.

In Fig. 3, we discussed the distinction in dynamics between rod glasses and gels. The packing and contact number ideas implicit in the Edwards and Evans model of the rod glass transition have been further explored by Philipse and co-workers.^{93,102,103} These results produce bounds on expected behavior in the (ϕ, r) space of Fig. 4. For example, the rod glass regime is bounded on the top by the maximum geometric packing fraction of isotropic rods,

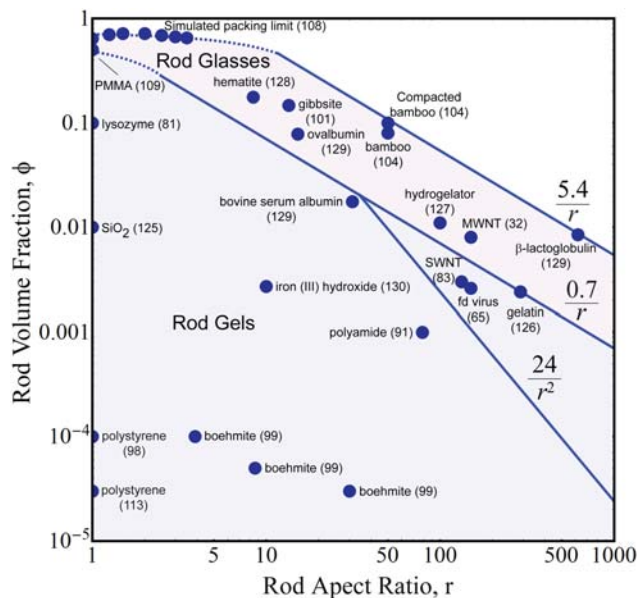


Fig. 4 Map of the volume fraction, aspect ratio space of rod suspensions, gels and glasses for which elasticity has been reported. Shown are data from a wide range of disciplines along with the relevant scaling relationships that bound the physical domains of rod dispersions.^{32,65,81,83,91,98,99,101,104,108,109,113,125–130} From top to bottom, the curves plotted are eqn (3)–(5) of the text.

$$\phi_{\max} \approx \frac{5.4}{r}, \quad (3)$$

as determined by scaling arguments combined with experimental results for granular rods.^{93,104} In addition, the isotropic–nematic transition for rods²⁴ closely tracks eqn (3)—the two lines differ by only a constant in the random contact theory. The microstructure of rod suspensions in the glass regime is that of the random homogeneous rod networks discussed in Fig. 2 and 3. This regime may include frictional granular structures.^{104,105}

The lower bound of the glass region may be taken as the minimum percolation volume fraction of a random homogeneous network of rods:

$$\phi_{\text{glass}} \approx \frac{0.7}{r} \quad (4)$$

determined by scaling and simulation^{102,106,107} and in suitable agreement with the Edwards and Evans⁹⁵ prediction of the dependence of the dynamical arrest volume fraction with aspect ratio ($C \approx 1$ in eqn (1)). Both eqn (3) and (4) arise from considering the random contact of rod pair excluded volumes and are thus valid in a high aspect ratio limit.

Eqn (3) and (4) plotted in Fig. 4 have been extended to low-aspect ratios, using dashed lines, to yield consistency with known spherical results. The upper limit of eqn (4) is extended by means of simulated prolate ellipsoid results,¹⁰⁸ and classical observations¹⁰⁹ have been used to extend the lower limit to $r = 1$. The lower dashed line also roughly agrees with theoretical and simulation results of the rod glass transition.^{110,111} However, the interesting non-monotonic behavior of random packing limits in the vicinity of $1 < r < 2$ suggests that these extrapolations be used with care in this aspect ratio range.^{108,112}

The region above eqn (3) does not admit packings with disordered structure. Alternatively, below the eqn (4) curve, rods are not sufficiently crowded to arrest due to excluded volume interactions alone and attractive interactions are required for the colloids to form a connected structure; the resultant heterogeneous structures may be fractals,⁷⁸ bundles,⁹¹ and other non-random shapes that might result, for example, from spinodal decomposition. Alternatively, if attractions are insufficiently strong, then below the eqn (4) boundary rod suspensions will display ergodicity and dispersed-phase rheology. Also shown on the plot is the semi-dilute limit for the dynamics of rod suspensions:⁴⁹

$$\phi_{\text{semi-dilute}} \approx \frac{24}{r^2} \quad (5)$$

This limit, which quantifies the region for which pair effects on suspension dynamics are observed, scales as the inverse of the aspect ratio squared. We note that denser structures like nematic and smectic liquid crystals (and, possibly, glasses of these structures) exist above the eqn (3) line and that the sharp boundaries represented by eqn (3)–(5) might be blurred by non-idealities such as rod semi-flexibility or polydispersity.

Eqn (3) and (4) group the available data in a useful way. First, none of the data falls above the eqn (3) limit. Second, many of the data cluster between the limits of eqn. (3) and (4). From the latter result, we may conclude that the generation of elasticity by the arrest of homogeneous fiber networks is widespread. The part of the diagram below eqn (4), which corresponds to low-volume

fraction gels formed by strong attractive interactions, is much less well populated. Nevertheless, it appears that by judicious design of attractive interactions, the lower region of Fig. 4 ought to be accessible. In fact, at the very bottom of the diagram, we expect to find a conceptual lower limit to the rod gel region. Below this limit the number concentration of rods would be insufficient to form a heterogeneous connected structure that could withstand either Brownian or gravitational stresses. Knowledge of such a limit would be economically relevant to production of, for example, cost-effective conducting networks of carbon nanotubes. A lower gelation limit was found for spheres by Manley *et al.*¹¹³ for density-matched latex colloids aggregated in microgravity into fractal gels: $\phi_{\text{sph,min}} \approx 3 \times 10^{-5}$. We would expect rods to display some such limit, though perhaps of a different magnitude. Although this conjecture has not yet been addressed, it has been observed that the degree of dynamical arrest of rod gels increases with aspect ratio at fixed volume fraction.⁹⁹ This result is consistent with the idea of a smaller minimum rod gelation limit for rods than for spheres. However, the lowest volume fraction rod gels we know of⁹⁹ are no lower than the limit found by Manley *et al.*¹¹³ Even if sphere and rod systems were found to possess similar minimum gelation thresholds, the magnitude of the contribution of rod to gel rheology appears to increase significantly with increasing aspect ratio at fixed volume fraction.^{26,86,101} Because the comparison between weak gels of rods and spheres is unclear, there is a need for systematic studies of these lower limits that assess aspect ratio effects and compare to literature results for spheres.

Most of the literature from which Fig. 4 was generated placed little emphasis on identifying the minimum volume fraction at which arrested dynamics occurred. Instead the concentrations reported were usually ones at which gelation was guaranteed. However, the economics of rod networks will increasingly drive optimization toward systems that minimize material usage. No matter the application focus, the gaps in Fig. 4 demonstrate the need for systematic study of the limits and complexity of the volume fraction–aspect ratio–pair potential phase space for arrested dynamics of rod systems.

6 Conclusions

Increasing the aspect ratio of a suspended colloid is a powerful means for fluid rheological modification that is used by nature, researcher, and industrialist alike. This review has focused on identifying the range of microstructures possible in rod suspensions and the implications of those microstructures for transitions in arrested dynamics and rheology. It appears that the field is somewhat fragmented and that interdisciplinary connections remain to be realized. Here we have highlighted areas of universality while acknowledging a range of unresolved questions of fundamental importance. Just as reported earlier for spheres, in which the nature of the arrested dynamics transition can vary from bonded gels (with heterogeneous fractal structure) to caged glasses (with homogeneous amorphous structure), so too may rods form structures that vary from homogeneous fiber networks—rod glasses—to heterogeneous fractal clusters—rod gels. The additional complexity addressed in this review is the effect of aspect ratio. At high aspect ratio, rod glasses may form due to caging and packing constraints at seemingly low-volume

fractions (e.g. ϕ_{glass} is as small as 0.02 at $r \approx 30$ as per Fig. 4). Here we have argued that rod suspensions may adopt a progression of structures and dynamics between the two limits of hard-rod packings and fractal clusters formed due to strong attractions. This progression from glass to gel in rods has received little fundamental attention. Yet, as shown in Fig. 4, it represents a large parameter space in which different types of arrested dynamics might well be generated through different combinations of volume fraction and aspect ratio.

As the field seeks to extend the state of the literature as summarized in this review, three directions are apparent. First, each datum point in Fig. 4 represents a gel or glass state generated by certain pair potential interactions (parameterized, for example, by $U_{\text{contact}}/k_{\text{B}}T$). Apart from the location of the hard-rod glass transition (which itself has not been completely identified), little is known of the magnitude of attractions required to generate the gel and glass states in the interior of Fig. 4. Second, even given knowledge of the location of gel and glass boundaries in Fig. 4, the rheological signatures that characterize them are largely unknown. The qualitatively different volume fraction and aspect ratio dependencies of local rod dynamics (cf. Fig. 3) suggest that gels and glasses will have quite different linear viscoelasticity. Third, the fundamentally different mechanisms for arrested dynamics in rod gels and glasses (bonding *versus* packing) and the very different microstructures (heterogeneous fractal clusters *versus* homogeneous fiber networks) suggest the hypothesis that non-linear rheological properties such as yield stress, shear thickening, and stress relaxation will vary profoundly within the parameter space delineated by Fig. 4.^{86,101,114,115}

Acknowledgements

We thank Dr Georgina Wilkins and Dr Pavlik Lettinga for discussions about this review, Bob Reeder for Fig. 1j and Stephanie Teich-McGoldrick for the preparation of Fig. 3a and b.

References

- O. Lieleg, K. M. Schmoller, C. J. Cyron, Y. Luan, W. A. Wall and A. R. Bausch, *Soft Matter*, 2009, **5**, 1796–1803.
- Y. C. Lin, G. H. Koenderink, F. C. MacKintosh and D. A. Weitz, *Macromolecules*, 2007, **40**, 7714–7720.
- L. A. Hough, M. F. Islam, P. A. Janmey and A. G. Yodh, *Phys. Rev. Lett.*, 2004, **93**, 168102–168101.
- B. Vigolo, C. Coulon, M. Maugey, C. Zakri and P. Poulin, *Science*, 2005, **309**, 920–923.
- J. R. Capadona, K. Shanmuganathan, D. J. Tyler, S. J. Rowan and K. Masschaele, *Science*, 2008, **319**, 1370–1374.
- C. F. Schmid, L. H. Switzer and D. J. Klingenberg, *J. Rheol. (N. Y.)*, 2000, **44**, 781–809.
- F. Ein-Mozaffari, C. P. J. Bennington and G. A. Dumont, *Chem. Eng. Sci.*, 2005, **60**, 2399–2408.
- S. G. Kim, J. W. Kim, W. H. Jang, H. J. Choi and M. S. Jhon, *Polymer*, 2001, **42**, 5005–5012.
- S. W. Ko, M. S. Yang and H. J. Choi, *Mater. Lett.*, 2009, **63**, 861–863.
- S. C. Glotzer and M. J. Solomon, *Nat. Mater.*, 2007, **6**, 557–562.
- M. A. Zirnsak, D. V. Boger and V. Tirtaatmadja, *J. Rheol. (N. Y.)*, 1999, **43**, 627–650.
- M. C. Yang, L. E. Scriven and C. W. Macosko, *J. Rheol. (N. Y.)*, 1986, **30**, 1015.
- T. M. Kwon, M. S. Jhon and H. J. Choi, *J. Mol. Liq.*, 1998, **75**, 115–126.
- H. J. Choi, T. M. Kwon and M. S. Jhon, *J. Mater. Sci.*, 2000, **35**, 889–894.
- R. G. Egres and N. J. Wagner, *J. Rheol. (N. Y.)*, 2005, **49**, 719–746.
- L. A. Cameron, T. M. Svitkina, D. Vignjevic, J. A. Theriot and G. G. Borisy, *Curr. Biol.*, 2001, **11**, 130–135.
- M. L. Gardel, J. H. Shin, F. C. MacKintosh, L. Mahadevan, P. A. Matsudaira and D. A. Weitz, *Phys. Rev. Lett.*, 2004, **93**, 188102.
- M. Doi and S. F. Edwards, *The Theory of Polymer Dynamics*, Clarendon Press, Oxford, 1986.
- F. Gittes and F. C. MacKintosh, *Phys. Rev. E: Stat. Phys., Plasmas, Fluids, Relat. Interdiscip. Top.*, 1998, **58**, R1241–R1244.
- D. C. Morse, *Phys. Rev. E: Stat. Phys., Plasmas, Fluids, Relat. Interdiscip. Top.*, 1998, **58**, R1237–R1240.
- J. Glaser, O. Hallatschek and K. Kroy, *Eur. Phys. J. E*, 2008, **26**, 123–136.
- M. Das, F. C. MacKintosh and A. J. Levine, *Phys. Rev. Lett.*, 2007, **99**, 038101.
- F. Hoffling, T. Munk, E. Frey and T. Franosch, *Phys. Rev. E: Stat. Phys., Plasmas, Fluids, Relat. Interdiscip. Top.*, 2008, **77**, 060904.
- L. Onsager, *Ann. N. Y. Acad. Sci.*, 1949, **51**, 627–659.
- Z. Dogic and S. Fraden, *Curr. Opin. Colloid Interface Sci.*, 2006, **11**, 47–55.
- A. Magnin and J. M. Piau, *J. Mater. Res.*, 1989, **4**, 990–995.
- L. A. Estroff and A. D. Hamilton, *Chem. Rev.*, 2004, **104**, 1201–1217.
- P. Terech, *Prog. Colloid Polym. Sci.*, 1996, **102**, 64–70.
- J. Liang, Y. Ma, Y. Zheng, H. T. Davis, H.-T. Chang, D. Binder, S. Abbas and F.-L. Hsu, *Langmuir*, 2001, **17**, 6447–6454.
- Rheox, Inc., *US Patent*, 5,340,390, 1994.
- P. Terech, V. Rodriguez, J. D. Barnes and G. B. McKenna, *Langmuir*, 1994, **10**, 3406–3418.
- Y. Y. Huang, S. V. Ahir and E. M. Terentjev, *Phys. Rev. B: Condens. Matter*, 2006, **73**, 125422–125421.
- J. S. Knutsen and M. W. Liberatore, *J. Rheol. (N. Y.)*, 2009, **53**, 877–892.
- J. Vermant and M. J. Solomon, *J. Phys.: Condens. Matter*, 2005, **17**, R1–R30.
- P. S. Russo, *Dynamic Light Scattering: The Method and Some Applications*, Oxford University Press, Oxford, 1995, pp. 512–553.
- D. H. Berry and W. B. Russel, *J. Fluid Mech.*, 1987, **180**, 475–494.
- J. D. Sherwood, *J. Fluid Mech.*, 1981, **111**, 347–366.
- J. K. G. Dhont and W. J. Briels, *Colloids Surf., A*, 2003, **213**, 131–156.
- R. M. Davis and W. B. Russel, *Macromolecules*, 1987, **20**, 518–525.
- V. Pryamitsyn and V. Ganesan, *J. Chem. Phys.*, 2008, **128**, 134901.
- Y. Mori, N. Ookubo and R. Hayakawa, *J. Polym. Sci., Part B: Polym. Phys.*, 1982, **20**, 2111–2124.
- C. J. S. Petrie, *J. Non-Newtonian Fluid Mech.*, 1999, **87**, 369–402.
- R. L. Powell, *J. Stat. Phys.*, 1991, **62**, 1073–1094.
- M. Rahnama, D. L. Koch and E. S. G. Shaqfeh, *Phys. Fluids*, 1995, **7**, 487–506.
- C. A. Stover, D. L. Koch and C. Cohen, *J. Fluid Mech.*, 1992, **238**, 277–296.
- E. S. G. Shaqfeh and G. H. Fredrickson, *Phys. Fluids A*, 1990, **2**, 7–24.
- I. L. Claeys and J. F. Brady, *J. Fluid Mech.*, 1993, **251**, 443–477.
- K. F. Wissbrun, *J. Rheol. (N. Y.)*, 1981, **25**, 619–662.
- R. G. Larson, *The Structure and Rheology of Complex Fluids*, Oxford University Press, New York, 1999.
- J. J. Magda, S. G. Baek, K. L. DeVries and R. G. Larson, *Macromolecules*, 1991, **24**, 4460–4468.
- W. R. Burghardt and G. G. Fuller, *Macromolecules*, 1991, **24**, 2546–2555.
- E. Zaccarelli, *J. Phys.: Condens. Matter*, 2007, **19**, 323101.
- V. Trappe and P. Sandkuhler, *Curr. Opin. Colloid Interface Sci.*, 2004, **8**, 494–500.
- E. K. Hobbie and D. J. Fry, *Phys. Rev. Lett.*, 2006, **97**, 036101.
- N. Fakhri, D. A. Tsybouski, L. Cognet, R. B. Weisman and M. Pasquali, *Proc. Natl. Acad. Sci. U. S. A.*, 2009, **106**, 14219–14223.
- M. J. Green, A. N. G. Parra-Vasquez, N. Behabtu and M. Pasquali, *J. Chem. Phys.*, 2009, **131**, 084901.
- A. Lucas, C. Zakri, M. Maugey, M. Pasquali, P. van der Schoot and P. Poulin, *J. Phys. Chem. C*, 2009, **113**, 20599–20605.

- 58 H. Wang, W. Zhou, D. L. Ho, K. I. Winey, J. E. Fischer, C. J. Glinka and E. K. Hobbie, *Nano Lett.*, 2004, **4**, 1789–1793.
- 59 C. Zakri and P. Poulin, *J. Mater. Chem.*, 2006, **16**, 4095–4098.
- 60 A. V. Kyrlyuk and P. van der Schoot, *Proc. Natl. Acad. Sci. U. S. A.*, 2008, **105**, 8221–8226.
- 61 D. Mukhija and M. J. Solomon, *J. Colloid Interface Sci.*, 2007, **314**, 98–106.
- 62 M. P. B. van Bruggen and H. N. W. Lekkerkerker, *Langmuir*, 2002, **18**, 7141–7145.
- 63 H. N. W. Lekkerkerker and A. Stroobants, *Nuovo Cimento Soc. Ital. Fis., D*, 1994, **16**, 949–962.
- 64 J. Buitenhuis, L. N. Donselaar, P. A. Buining, A. Stoobants and H. N. K. Lekkerkerker, *J. Colloid Interface Sci.*, 1995, **175**, 46–56.
- 65 Z. K. Zhang, N. Krishna, M. P. Lettinga, J. Vermant and E. Grelet, *Langmuir*, 2009, **25**, 2437–2442.
- 66 F. Huang, R. Rotstein, S. Fraden, K. E. Kasza and N. T. Flynn, *Soft Matter*, 2009, **5**, 2766–2771.
- 67 P. G. Bolhuis, A. Stroobants, D. Frenkel and H. N. W. Lekkerkerker, *J. Chem. Phys.*, 1997, **107**, 1551–1564.
- 68 P. Bolhuis and D. Frenkel, *J. Chem. Phys.*, 1997, **106**, 666–687.
- 69 D. Frenkel and B. M. Mulder, *Mol. Phys.*, 1985, **55**, 1171–1192.
- 70 I. Langmuir, *J. Chem. Phys.*, 1938, **6**, 873–896.
- 71 G. J. Vroege and H. N. W. Lekkerkerker, *Rep. Prog. Phys.*, 1992, **55**, 1241–1309.
- 72 D. Frenkel, H. N. W. Lekkerkerker and A. Stroobants, *Nature*, 1988, **332**, 822–823.
- 73 E. Grelet, *Phys. Rev. Lett.*, 2008, **100**, 168301.
- 74 P. Denking and W. Burchard, *J. Polym. Sci., Part B: Polym. Phys.*, 1991, **29**, 589–600.
- 75 R. Duggal and M. Pasquali, *Phys. Rev. Lett.*, 2006, **96**, 246104.
- 76 E. de Miguel, L. F. Rull, M. K. Chalam and K. E. Gubbins, *Mol. Phys.*, 1991, **72**, 593–605.
- 77 Z. Dogic, K. R. Purdy, E. Grelet, M. Adams and S. Fraden, *Phys. Rev. E: Stat. Phys., Plasmas, Fluids, Relat. Interdiscip. Top.*, 2004, **69**, 051702.
- 78 A. Mohraz, D. B. Moler, R. M. Ziff and M. J. Solomon, *Phys. Rev. Lett.*, 2004, **92**, 155503.
- 79 H. C. van de Hulst, *Light Scattering by Small Particles*, Dover, New York, 1981.
- 80 R. S. Justice, D. H. Wang, L. S. Tan and D. W. Schaefer, *J. Appl. Crystallogr.*, 2007, **40**, S88–S92.
- 81 P. Schurtenberger, L. J. Magid, S. M. King and P. Lindner, *J. Phys. Chem.*, 1991, **95**, 4173–4176.
- 82 L. M. DeLong and P. S. Russo, *Macromolecules*, 1991, **24**, 6139–6155.
- 83 L. A. Hough, M. F. Islam, B. Hammouda, A. G. Yodh and P. A. Heiney, *Nano Lett.*, 2006, **6**, 313–317.
- 84 T. Chatterjee, A. Jackson and R. Krishnamoorti, *J. Am. Chem. Soc.*, 2008, **130**, 6934–6935.
- 85 B. J. Bauer, E. K. Hobbie and M. L. Becker, *Macromolecules*, 2006, **39**, 2637–2642.
- 86 A. Wierenga, A. P. Philipse and H. N. W. Lekkerkerker, *Langmuir*, 1998, **14**, 55–56.
- 87 W. Zhou, M. F. Islam, H. Wang, D. L. Ho, A. G. Yodh, K. I. Winey and J. E. Fischer, *Chem. Phys. Lett.*, 2004, **384**, 185–189.
- 88 S. H. Chen and J. Teixeira, *Phys. Rev. Lett.*, 1986, **57**, 2583–2586.
- 89 M. Carpineti and M. Giglio, *Phys. Rev. Lett.*, 1992, **68**, 3327–3330.
- 90 M. P. Lettinga, K. Kang, A. Imhof, D. Derks and J. K. G. Dhont, *J. Phys.: Condens. Matter*, 2005, **17**, S3609–S3618.
- 91 G. M. H. Wilkins, P. T. Spicer and M. J. Solomon, *Langmuir*, 2009, **25**, 8951–8959.
- 92 T. G. Mason and D. A. Weitz, *Phys. Rev. Lett.*, 1995, **74**, 1250–1253.
- 93 A. P. Philipse, *Langmuir*, 1996, **12**, 1127–1133; *cf.*, Corrigendum, 1996, **12**, 5971.
- 94 T. Munk, F. Hofling, E. Frey and T. Franosch, *Europhys. Lett.*, 2009, **85**, 30003.
- 95 S. F. Edwards and K. E. Evans, *J. Chem. Soc., Faraday Trans. 2*, 1982, **78**, 113–121.
- 96 T. Schilling, S. Jungblut and M. A. Miller, *Phys. Rev. Lett.*, 2007, **98**, 108303.
- 97 P. N. Pusey and W. van Meegen, *Physica A (Amsterdam)*, 1989, **157**, 705–741.
- 98 A. H. Krall and D. A. Weitz, *Phys. Rev. Lett.*, 1998, **80**, 778–781.
- 99 A. Mohraz and M. J. Solomon, *J. Colloid Interface Sci.*, 2006, **300**, 155–162.
- 100 A. A. Gusev, *Macromolecules*, 2001, **34**, 3081–3093.
- 101 A. J. W. ten Brinke, L. Bailey, H. N. W. Lekkerkerker and G. C. Maitland, *Soft Matter*, 2007, **3**, 1145–1162.
- 102 A. P. Philipse and A. Wierenga, *Langmuir*, 1998, **14**, 49–54.
- 103 A. Wouterse, S. R. Williams and A. P. Philipse, *J. Phys.: Condens. Matter*, 2007, **19**, 406215.
- 104 J. Blouwolff and S. Fraden, *Europhys. Lett.*, 2006, **76**, 1095–1101.
- 105 W. N. Man, A. Donev, F. H. Stillinger, M. T. Sullivan, W. B. Russel, D. Heeger, S. Inati, S. Torquato and P. M. Chaikin, *Phys. Rev. Lett.*, 2005, **94**, 198001.
- 106 I. Balberg and N. Binenbaum, *Phys. Rev. A*, 1987, **35**, 5174.
- 107 E. J. Garboczi, K. A. Snyder, J. F. Douglas and M. F. Thorpe, *Phys. Rev. E: Stat. Phys., Plasmas, Fluids, Relat. Interdiscip. Top.*, 1995, **52**, 819.
- 108 A. Donev, I. Cisse, D. Sachs, E. A. Variano, F. H. Stillinger, R. Connelly, S. Torquato and P. M. Chaikin, *Science*, 2004, **303**, 990–993.
- 109 P. N. Pusey and W. van Meegen, *Nature*, 1986, **320**, 340–342.
- 110 G. Yatsenko and K. S. Schweizer, *Langmuir*, 2008, **24**, 7474–7484.
- 111 P. Pfeiderer, K. Milinkovic and T. Schilling, *Europhys. Lett.*, 2008, **84**, 16003.
- 112 S. Sacanna, L. Rossi, A. Wouterse and A. P. Philipse, *J. Phys.: Condens. Matter*, 2007, **19**, 376108.
- 113 S. Manley, L. Cipelletti, V. Trappe, A. E. Bailey, R. J. Christianson, U. Gasser, V. Prasad, P. N. Segre, M. P. Doherty, S. Sankaran, A. L. Jankovsky, B. Shiley, J. Bowen, J. Eggers, C. Kurta, T. Lorik and A. D. Weitz, *Phys. Rev. Lett.*, 2004, **93**, 108302–108302.
- 114 R. G. Egres, F. Nettekheim and N. J. Wagner, *J. Rheol. (N. Y.)*, 2006, **50**, 685–709.
- 115 A. J. W. ten Brinke, L. Bailey, H. N. W. Lekkerkerker and G. C. Maitland, *Soft Matter*, 2008, **4**, 337–348.
- 116 M. G. Basavaraj, G. G. Fuller, J. Fransaeer and J. Vermant, *Langmuir*, 2006, **22**, 6605–6612.
- 117 R. J. Bird and G. Rooney, *Nature*, 1961, **190**, 337–338.
- 118 L. Howard, http://commons.wikimedia.org/wiki/File:Fibers_of_Collagen_Type_I_-_TEM.jpg, last accessed 23 January 2010.
- 119 X. Y. Liu, P. D. Sawant, W. B. Tan, I. B. M. Noor, C. Pramesti and B. H. Chen, *J. Am. Chem. Soc.*, 2002, **124**, 15055–15063.
- 120 C. J. Murphy, T. K. Sau, M. Gole Anand, J. Orendorff Christopher, J. Gao, L. Gou, E. Hunyadi Simona and T. Li, *J. Phys. Chem. B*, 2005, **109**, 13857–13870.
- 121 M. Ozaki, S. Kratochvil and E. Matijevic, *J. Colloid Interface Sci.*, 1984, **102**, 146–151.
- 122 P. Simon, H. Lichte, P. Formanek, M. Lehmann, R. Huhle, W. Carrillo-Cabrera, A. Harscher and H. Ehrlich, *Micron*, 2008, **39**, 229–256.
- 123 P. Terech and R. G. Weiss, *Chem. Rev.*, 1997, **97**, 3133–3159.
- 124 M. P. B. Van Bruggen, *Langmuir*, 1998, **14**, 2245–2255.
- 125 M. C. Grant and W. B. Russel, *Phys. Rev. E: Stat. Phys., Plasmas, Fluids, Relat. Interdiscip. Top.*, 1993, **47**, 2606.
- 126 C. Joly-Duhamel, D. Hellio, A. Ajdari and M. Djabourov, *Langmuir*, 2002, **18**, 7158–7166.
- 127 N. M. Sangeetha, S. Bhat, U. Maitra and P. Terech, *J. Phys. Chem. B*, 2004, **108**, 16056–16063.
- 128 M. J. Solomon and D. V. Boger, *J. Rheol. (N. Y.)*, 1998, **42**, 929–949.
- 129 C. Veerman, L. M. C. Sagis and E. van der Linden, *Spec. Publ. - R. Soc. Chem.*, 2005, **298**, 247–255.
- 130 M. Zrinyi, M. Kabai-Faix, F. Horkay and S. Fuhos, *Langmuir*, 1993, **9**, 71–76.